Development and experiment of the mechanism for oolong tea stirring motion based on the manual stirring characteristics analysis

Jianneng Chen[1,2], Kun Yao[1], Binsong Zhou[1], Xiong Zhao[1,2], Xianbing Bian[1], Zheng Zhu[1], Jiangming Jia[1,2*]

(1. *School of Mechanical Engineering, Zhejiang Sci-Tech University, Hangzhou 310018, China*;
2. *Key Laboratory of Transplanting Equipment and Technology of Zhejiang Province, Hangzhou 310018, China*)

Abstract: In this study, the motion characteristics of manual stirring were analyzed to achieve the goal of realizing a high-quality mechanized imitation of manual stirring for oolong tea. A test bench for collecting the motion characteristics of manual stirring was designed, and the standard manual stirring motion characteristic curve was obtained. According to the requirements of the stirring motion characteristics, a variable-speed and variable-amplitude stirring mechanism was proposed, the kinematics model and reverse design model of the stirring mechanism were established, auxiliary analysis and design software were written, and the non-circular gear pitch curve and cam profile curve were obtained. A three-dimensional model of the stirring machine was established, a virtual prototype of the stirring machine was built, and the simulation experiment was completed by using the ADAMS software. A prototype of the stirring machine was developed, and the stirring experiment was conducted on the prototype. The maximum deviation of the pitch angle is 2.8772°, and the maximum deviation of the roll angle is 1.5948° according to the analysis and comparison of the actual curve data and the theoretical data curve. The experimental results showed that the simulation angle curve and the actual angle curve were consistent with the theoretical standard manual stirring motion characteristic curve, which verified the correctness of the design and modeling of the stirring mechanism. The tea was mechanically stirred by the stirring mechanism to achieve the desired stirring effect, which verified the feasibility of the stirring machine.

Keywords: oolong tea, manual stirring, stirring motion, stirring mechanism, reverse design
DOI: 10.25165/j.ijabe.20231605.7524

Citation: Chen J N, Yao K, Zhou B S, Zhao X, Bian X B, Zhu Z, et al. Development and experiment of the mechanism for oolong tea stirring motion based on the manual stirring characteristics analysis. Int J Agric & Biol Eng, 2023; 16(5): 260–269.

1 Introduction

Stirring is the key process to form the unique aroma and taste of oolong tea, which is essential to ensure the tea's quality[1-3]. Stirring allows the tea to move in three dimensions in the bamboo sieve so that relative motions, such as beating, rotation, and friction, are carried out between the tea leaves. At present, the common stirring methods involve manual and mechanical stirring[4]. Manual stirring moves the tea evenly on the bamboo sieve; hence, the quality of the tea is good. However, the labor intensity is high, hindering the ability to meet the demand for mass production of oolong tea. To reduce the stirring labor intensity, special machinery has been implemented to stir the tea.

The tea roller stirring machine[5] is the most common equipment for stirring at present. It uses the friction of the barrel wall to bring the tea to a certain height and then throws the leaves down, causing them to rub and collide to achieve stirring. However, due to the different heights of the tea being lifted by the barrel wall, the length of the falling stroke is different, and the force of the tea is uneven, so the uniformity of the obtained tea is poor[6]. Hao et al.[7] designed oolong tea vibration stirring equipment, which can realize tea vibration stirring through an eccentric slider device. However, the trajectory of the tea motion driven by this device is different from the three-dimensional motion of manual stirring. There is only a simple two-dimensional motion, so the interaction between the tea leaves is limited. Cheng et al.[8] invented a hand-sieve-type tea stirring machine that can imitate manual stirring action to stir tea. However, due to the fixed motor speed and sieve inclination, the speed change of the tea is small; hence, the stirring effect is poor. Yang et al.[9] designed a spherical type of tea stirring machine that can realize 360° tea stirring without dead corners. However, the tea is brought to a high level during stirring, and the impact force received by the tea is large, so a similar problem to that of the tea roller stirring machine arises; the tea is easily damaged, and the stirring quality is not good. To summarize, the current stirring equipment has problems, such as poor stirring uniformity and insufficient relative motion of the tea, resulting in low-quality tea. Therefore, it is important to design a tea stirring machine that meets the characteristics of manual stirring to achieve uniform and sufficient relative motion of tea.

In this study, the motion characteristics of manual stirring were analyzed and collected. Furthermore, a new type of variable-speed and variable-amplitude stirring mechanism was proposed, which can implement the motion of a bamboo sieve with variable speed

Received date: 2022-03-18 **Accepted date:** 2022-11-14
Biographies: Jianneng Chen, PhD, Professor, research interest: agricultural machinery equipment and technology, Email: jiannengchen@zstu.edu.cn; **Kun Yao**, PhD, research interest: design and optimization of agricultural machinery, Email: 1592553951@qq.com; **Binsong Zhou**, MS, research interest: design and optimization of agricultural machinery, Email: 770120752@qq.com; **Xiong Zhao**, PhD, Associate professor, research interest: research and development of intelligent agricultural equipment, Email: zhaoxiong@zstu.edu.cn; **Xianbing Bian**, MS, research interest: design and optimization of agricultural machinery, Email: 850792774@qq.com; **Zheng Zhu**, MS, research interest: design and optimization of agricultural machinery, Email: 429189077@qq.com.
***Corresponding author: Jiangming Jia**, PhD, Assistant Professor, research interest: design and optimization of agricultural machinery. Faculty of Mechanical Engineering & Automation, Zhejiang Sci-Tech University, Hangzhou, 310018, China. Tel: +86-13705810950, Email: jarky@zstu.edu.cn.

and variable inclination. A mathematical model was established to reverse engineer the parameters of the mechanism from the manual stirring motion characteristics, and auxiliary analysis and design software were written to establish the non-circular gear pitch curve and cam profile curve of the mechanism. Finally, three-dimensional modeling, virtual simulation, and experiments with the stirring mechanism were carried out to verify the feasibility of the stirring mechanism.

2 Analysis and collection of standard manual stirring motion characteristics

2.1 Analysis of manual stirring motion characteristics

Traditional manual stirring is usually carried out on a hanging sieve. The tea master controls the hoisted bamboo sieve to shake in space with both hands, driving the tea in the sieve to roll and jump to achieve stirring. In this study, manual stirring in Anxi, Fujian, China, was investigated, and the stirring motion characteristics were analyzed.

To describe the motion characteristics of the sieve during stirring, this study referenced the definition of the attitude angle[10-12] in aviation and defined the attitude description method of the bamboo sieve in combination with actual needs. The world coordinate system A and sieve reference system B are defined as shown in Figure 1. In the beginning, the two coordinate systems coincide. Coordinate system B first rotates γ around the Y-axis of coordinate system A, then rotates θ around the X-axis of coordinate system A, and finally rotates Ψ around the Z-axis of coordinate system A similar to the actual attitude of the bamboo sieve. The rotation angles of coordinate system B around the three X-Y-Z axes are the attitude angles of the sieve, which are called the pitch angle, roll angle, and yaw angle. By obtaining the attitude angle and the coordinates of the sieve center point, the pose of the sieve can be described.

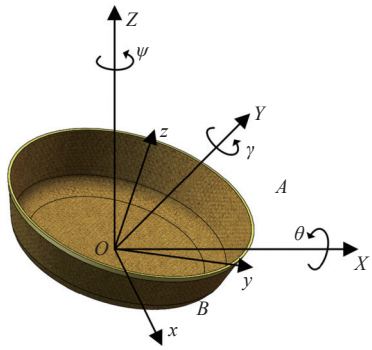

Figure 1 Coordinate system definition

The motion characteristics of the sieve in manual stirring were analyzed by observing the actions of the tea master and the motion of the sieve. During the stirring process, the inclination angle and the shaking speed of the bamboo sieve change continually, and the sieve undergoes a three-dimensional variable-speed motion. The inertial force generated by the variable-speed motion causes the tea to roll and rub in the sieve. Under the constraint of ropes, the sieve moves on a conical surface in space. The sieve always faces outward, while the central axis of the sieve approximately passes through a certain point below the sieve. This point is defined as the cone apex point of the conical surface motion. The sieve does not rotate when manually stirring, so the yaw angle can be ignored. Combining the previous definition of the sieve attitude, the attitude angle required to describe the attitude of the sieve can be reduced to two, just the pitch angle and the roll angle.

Based on the above characteristics, the summary of the motion characteristics of manual stirring is as follows:

1) The inclination angle and shaking speed of the sieve constantly change during the stirring process;

2) The shaking of the sieve can be approximately regarded as the motion of the sieve around the cone apex point;

3) There is no rotation in the motion of the sieve, so only two attitude angles can describe the attitude.

2.2 Design of the test bench for collecting the motion characteristics of manual stirring

It is difficult to directly collect the motion characteristic data of the sieve during manual stirring, so a special test bench was designed to obtain the stirring motion characteristics.

As shown in Figure 2, the test bench is mainly composed of a fixed frame, a shaking frame, a bearing set, a sieve shaft, a hall angle sensor, and a bamboo sieve. The shaking frame is supported by a set of bearing seats installed on the frame and can rotate around the x-axis, whereas the sieve shaft is supported by a pair of bearings installed on the shaking frame and can rotate around the y-axis. Through the vertically installed bearings, the sieve shaft can rotate around the x-axis and y-axis at the same time, and the intersection of the two rotation axes is the cone apex point of the sieve cone motion. On the test bench, the center point of the sieve can make a spherical motion with the cone apex point at the center of the sphere. Therefore, the inclination angle of the sieve can be changed freely during the stirring process. Moreover, the shaking speed can also be freely controlled. Combined with the definition of the attitude angle of the sieve, the pitch angle and roll angle of the sieve are the rotation angles of the sieve around the x-axis and y-axis. Therefore, a hall angle sensor was installed at the shaft ends to obtain the rotation angle data of these two axes. The length of the sieve shaft and the cone apex point of motion are known, so the position of the sieve center point is a known quantity. In summary, the test bench for collecting the motion characteristics of the stirring motion only needs to collect the rotation angle data of the two rotating shafts to obtain the posture change of the sieve during the stirring process. Although the structure of the test bench is different from that of rope stirring, it can complete the variable speed and amplitude motion required by manual stirring and realize the cone motion of the sieve around the cone apex point, which basically restores the important motion characteristics of the rope stirring proposed in the previous section. Therefore, it can accurately collect the motion characteristics of manual stirring. The data acquisition module of the test bench was controlled by the Arduino Mega 2560 development board, the rotation angle was acquired by a Hall angle sensor, and the sampled angle data were read and stored by a PC.

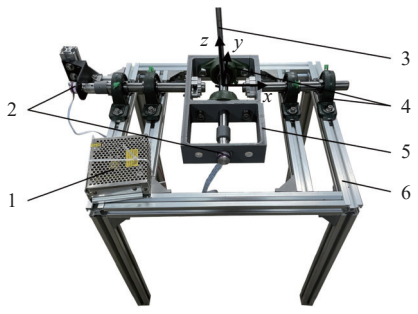

1. Switching power supply 2. Hall angle sensor 3. Sieve shaft 4. Bearing set 5. Shaking frame 6. Frame

Figure 2 Manual stirring motion characteristics acquisition test bench

2.3 Acquisition of standard manual stirring motion characteristics based on a three-dimensional Fourier series

Based on the established acquisition test bench, the manual stirring motion characteristics were collected. The angle sensor performed angle correction first, and then manual stirring was carried out on the test bench, as shown in Figure 3. Several sets of rotation angle data consisting of different pitch and roll angles were collected, as shown in Figure 4.

Figure 3 Schematic diagram of stirring on the test bench

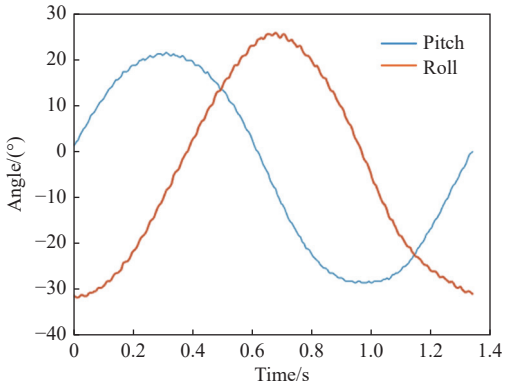

Figure 4 Schematic diagram of the sampled stirring data

The rotation angles of the two shafts were only an indirect manifestation of the sieve pose. Therefore, the stirring data were further processed, and the description of the pose of the sieve was simplified as a point plus line to better reflect the motion characteristics of the sieve. As shown in Figure 5, the center of the sieve moves on the spherical surface with the cone apex point O at the center of the sphere. Let OP be the sieve shaft at a certain time; then, OP can be regarded as obtained by rotating the vertical sieve shaft OM around the Y-axis γ and then around the X-axis θ in the initial state. The pose of the sieve at a certain time can be represented by a point P and a line OP. Through the rotation matrix, the rotation angle information collected by the sensor can be converted into the pose information of the sieve.

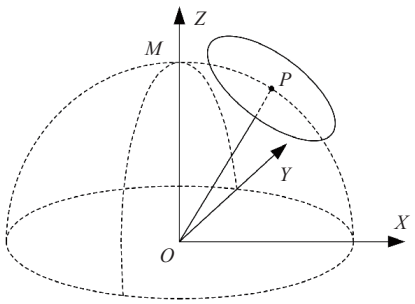

Figure 5 Rotation of the sieve shaft

Given that the length of the sieve shaft is l_0 (mm), the coordinates of point P are as follows:

$$\begin{bmatrix} P_x \\ P_y \\ P_z \end{bmatrix} = R_x \cdot R_y \cdot \begin{bmatrix} 0 \\ 0 \\ l_0 \end{bmatrix} \tag{1}$$

where, P_x, P_y, and P_z are the X, Y, and Z coordinates of point P. R_x is the rotation matrix around the X-axis and R_y is the rotation matrix around the Y-axis. The expressions of R_x and R_y are as follows:

$$R_x = \begin{bmatrix} 1 & 0 & 0 \\ 0 & \cos\theta & -\sin\theta \\ 0 & \sin\theta & \cos\theta \end{bmatrix} \tag{2}$$

$$R_y = \begin{bmatrix} \cos\gamma & 0 & \sin\gamma \\ 0 & 1 & 0 \\ \sin\gamma & 0 & \cos\gamma \end{bmatrix} \tag{3}$$

The collected rotation angle data were calculated by using Equation (1) to obtain the coordinate change of sieve center point P in the stirring process. Then, the connecting line between point O and point P forms the attitude of the sieve. Figure 6 shows a group of calculated poses of a sieve, where the line represents the attitude of the sieve, and the asterisk represents the position of the center point of the sieve. Figure 6 shows that there are fluctuations in the sampling rotation angle; hence, the connection of the sieve center point is not smooth, and it is not conducive to the subsequent reverse calculation of the mechanism. Therefore, data need to be fitted[13-15], and a three-dimensional Fourier series was used to smoothly fit the center point of the sieve.

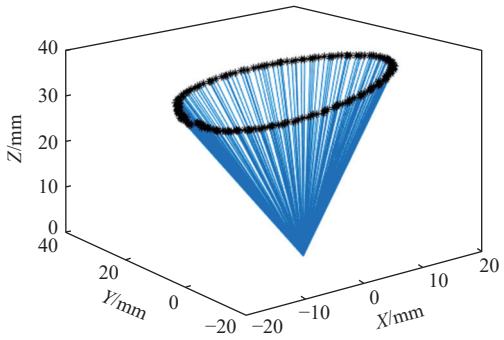

Figure 6 Pose of the sieve obtained from the rotation angle.

A periodic function can be represented as the sum of a constant value and an infinite number of harmonic components of different frequencies of the Fourier series[16,17]. In three-dimensional space, a three-dimensional closed space curve $F(\omega)$ can be expressed by Equation (4), where x, y, and z in Equation (4) are the x, y, and z coordinates of the curve, respectively.

$$F(\omega) = ix(\omega) + jy(\omega) + kz(\omega) \tag{4}$$

When the input is uniformly rotated, Equation (4) can be rewritten as follows:

$$F(t) = ix(t) + jy(t) + kz(t) \tag{5}$$

Equation (5) can be expressed according to a one-dimensional Fourier series (X-axis) and a two-dimensional Fourier series (OYZ plane) as follows:

$$F_{px}(t) = \sum_{n=-\infty}^{+\infty} c_n e^{i\varphi_n} e^{in\omega t} \tag{6}$$

$$F_{pyz}(t)=\sum_{n=-\infty}^{+\infty}c'_n e^{i\varphi'_n}e^{in\omega t} \tag{7}$$

In Equations (6) and (7), c_n is the amplitude of the n^{th} harmonic component, and φ_n is the phase of the n^{th} harmonic component.

The fast Fourier transform can be used to calculate the Fourier coefficient corresponding to the discrete value of the sieve center point, and the amplitude c_n and phase φ_n can be separated.

The expression of the three-dimensional Fourier series[18,19] for the center point of the sieve is as follows:

$$\begin{aligned}F(t)=\sum_{n=1}^{\infty}[&(iR_0\cos\phi_0+jR_0\sin\phi_0\cos\psi_0+kR_0\sin\phi_0\sin\psi_0)+\\&i(R_n\cos\phi_n+R_{-n}\cos\phi_{-n})+j(R_n\sin\phi_n\cos\psi_n+\\&R_{-n}\sin\phi_{-n}\cos\psi_{-n})+k(R_n\sin\phi_n\sin\psi_n+R_{-n}\sin\phi_{-n}\sin\psi_{-n})]\end{aligned} \tag{8}$$

In Equation (8), $R_n=\sqrt{c_n^2+c_n'^2}\ n=0,1,2,\ldots;$

$\phi_n=\arccos(c_n\cos(\varphi_n+n\omega t)/R_n)n=0,1,2,\ldots;$

$\psi_n=\arctan(R_{nz}/R_{ny})n=0,1,2,\ldots;$

$R_{ny}=c_n|\sin(\varphi_n+n\omega t)|\sin(\varphi'_n+n\omega t)+c'_n\cos(\varphi'_n+n\omega t);$

$R_{nz}=-c_n|\sin(\varphi_n+n\omega t)|\cos(\varphi'_n+n\omega t)+c'_n\sin(\varphi'_n+n\omega t);$

$R_{-n}=\sqrt{c_{-n}^2+c_{-n}'^2-2c_{-n}c'_{-n}|\sin(\varphi_{-n}-n\omega t)|\sin(\varphi'_n-\varphi'_{-n}+2n\omega t)};$

$\phi_{-n}=\arccos(c_{-n}\cos(\varphi_{-n}-n\omega t)/R_{-n})n=1,2,\ldots;$

$\psi_{-n}=\arctan(R_{-nz}/R_{-ny})n=1,2,\ldots;$

$R_{-ny}=-c_{-n}|\sin(\varphi_{-n}-n\omega t)|\sin(\varphi'_n+n\omega t)+c'_{-n}\cos(\varphi'_{-n}-n\omega t);$

$R_{-nz}=c_{-n}|\sin(\varphi_{-n}-n\omega t)|\cos(\varphi'_n+n\omega t)+c'_{-n}\sin(\varphi'_{-n}-n\omega t).$

In the equation above, R_n and R_{-n} represent the amplitude of the n^{th} term of the harmonic components of the positive and negative terms, respectively; ϕ_n and ϕ_{-n} represent the angle between R_n, R_{-n} and the x-axis, respectively; and Ψ_n and Ψ_{-n} represent the angle between the projection of R_n and R_{-n} on the OYZ plane and the y-axis, respectively.

Although in theory, the curve needs infinite harmonic components to fit, in engineering, the Fourier series only needs a limited number of harmonic components to meet the actual needs. Based on the three-dimensional Fourier series, 5 harmonic components are taken for fitting, and the fitting effect is shown in Figure 7 below. The asterisk in the figure represents the raw data, and the square represents the data that have been fitted. After fitting the three-dimensional Fourier series, the fluctuating discrete points become smooth, and the center point of the sieve has the corresponding fitting mathematical expression.

Several sets of stirring data were sampled, with a different number of sampling points in each group. To obtain the standard stirring motion characteristics, the calculated sieve center point trajectory expression was directly interpolated, the number of data points in each group was expanded to 360, and the average value was calculated. Considering that the input would rotate at a constant speed, to facilitate subsequent analysis, the rotation angle relationship was changed from time-related to rotation angle-related, and the standard stirring motion characteristics were obtained, as shown in Figure 8. The subsequent mechanism design was based on the standard stirring motion characteristics.

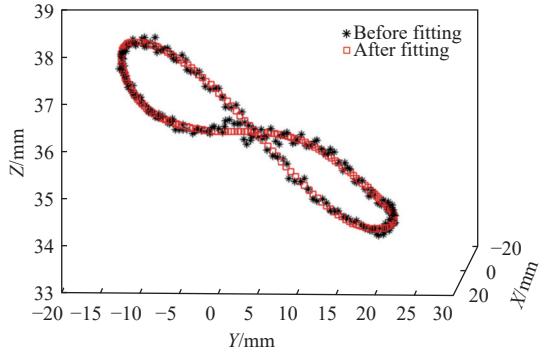

Figure 7 Fourier series fitting effect

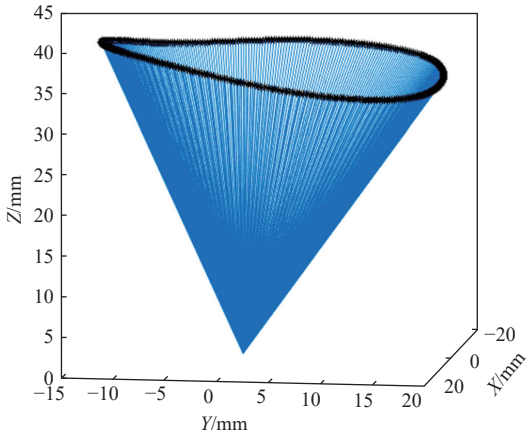

a. Sieve pose under standard stirring motion

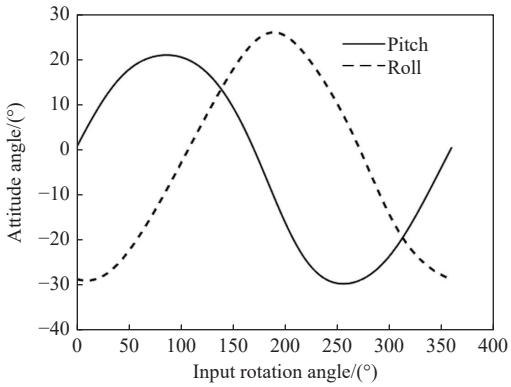

b. Rotation angles under standard stirring motion

Figure 8 Standard stirring motion characteristics

3 Scheme design of the variable-speed and variable-amplitude stirring mechanism

Figure 8 shows that the hand-sieve type stirring machine needs to move at a variable speed; however, the hand-sieve type stirring machine currently on the market is at a constant speed[7-9], so it cannot achieve the effect of manual stirring. In this study, the innovative design of the mechanism is implemented based on the obtained manual stirring motion characteristics.

In actual manual stirring, the sieve makes spatial shaking with variable speed and amplitude, and the shaking can be approximately regarded to be around a certain cone apex point below the sieve. The structure of the stirring test bench designed above can be used as the frame of the subsequent stirring machine to provide the cone apex point required for stirring. Taking the cone apex point of the

mechanism as the fixed point and the endpoint of the sieve shaft as the moving point, a straight line can be determined at these two points. Since the sieve does not rotate, these two points can determine the sieve's two attitude angles in space. To obtain the sieve's motion characteristics, the reproduction of the stirring action can be achieved by restricting the motion of the end of the sieve shaft.

A variable-speed and variable-amplitude stirring mechanism was designed, as shown in Figure 9. The transmission principle of the mechanism is as follows. The motor drives the input shaft to rotate at a constant speed and drives the non-circular gear[20-24] to rotate so that the main shaft rotates at a variable speed according to the design requirements. The main shaft is fixedly connected to the bottom plate to be able to rotate the bottom plate and drive the planetary gear to revolve and rotate around the sun gear. Driven by the planetary gear, the cam fixed to the drive shaft rotates, which in turn drives the slider to move. A fixed spherical hinge on the slider cooperates with the fixed cone apex point to drive the sieve to shake in space. This mechanism can change the amplitude and speed of the sieve in the stirring process. The spherical hinge fixed to the slider is the moving point. The movement of the slider can be controlled by designing the cam shape to control the inclination of the sieve. The non-circular gear can output a designed variable speed motion. By controlling the rotation speed of the main shaft, the rotation speed and the shaking speed of the planetary gear and the sieve are also controlled.

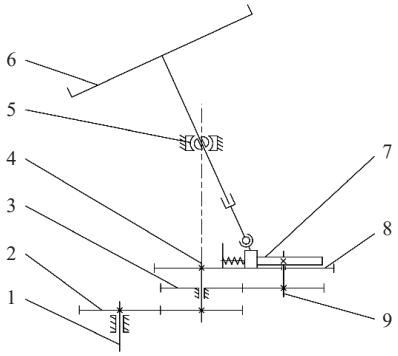

1. Input shaft 2. Non-circular gear set 3. Planetary gear train 4. Main shaft 5. Cone apex 6. Bamboo sieve 7. Cam slider 8. Bottom plate 9. Transmission shaft

Figure 9 Schematic diagram of the variable-speed and variable-amplitude stirring mechanism

4 Kinematic model establishment and reverse design of the stirring mechanism

4.1 Kinematic model establishment of the stirring mechanism

To better establish the kinematic model of the mechanism, the stirring mechanism is simplified, and only the most important part of the mechanism is shown, as seen in Figure 10. The *OP* rod in the figure shows the distance from the spherical hinge to the centerline of the main shaft, and its length is controlled by the cam. Point *Q* is the cone apex point of the mechanism, and point *K* is the center point of the sieve. When point *P* makes a circular motion around the origin *O*, the attitude of straight-line *PK* changes continuously. The speed of *OP* is controlled by the non-circular gear, which makes a variable speed motion.

The model simplifies the parts of the cam slider and non-circular gears. If the input member of the mechanism rotates at a uniform angular speed ω , the relationship between the rotation angle φ_1 of the driving wheel of the non-circular

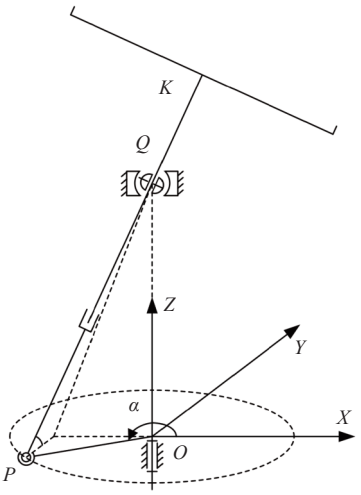

Figure 10 Schematic diagram of the mechanism kinematic model

gear and the time *t* is $\varphi_1=\omega t$. The rotation angle φ_2 of the driven wheel is related to φ_1, and the relationship is $\varphi_2=F(\varphi_1)$. The bottom plate is fixed to the driven wheel, and the rotation angle α of the *OP* is equal to φ_2, which is also related to the rotation angle φ_1 of the driving wheel. The length l_1 of the *OP* rod is related to the rotation angle of the cam, and the rotation angle of the cam is equal to the rotation angle of the planetary gear. In the designed planetary gear system, the gear ratio of the sun gear to the planetary gear is 1:1, so the cam rotation angle is equal to the non-circular follower rotation angle φ_2. Hence, l_1 is related to φ_2; in fact, it is also related to φ_1, denoted as $l_1(\varphi_1)$. In conclusion, the effects of cam sliders and non-circular gears can be directly replaced by changes in rotation angle $\alpha(\varphi_1)$ and length $l_1(\varphi_1)$ of the *OP*.

In Figure 10, the closed vector equation of robs is established according to the closed space figure *OPK* as follows:

$$\boldsymbol{l}_{OP}+\boldsymbol{l}_{PK}+\boldsymbol{l}_{KO}=\boldsymbol{0} \tag{9}$$

Point *P* moves on the *OXY* plane, and the coordinates of crank end point *P* are expressed in Equation (10).

$$\begin{cases} P_x=l_1(\varphi_1)\cos\alpha \\ P_y=l_1(\varphi_1)\sin\alpha \\ P_z=0 \end{cases} \tag{10}$$

Suppose the height of the cone apex point *Q* is *h* and its coordinate is (0, 0, *h*); then, the vector $\boldsymbol{l}_{PQ}$ is

$$\boldsymbol{l}_{PQ}=\boldsymbol{l}_{OQ}-\boldsymbol{l}_{OP}=(-P_x,-P_y,h) \tag{11}$$

The straight-line *PQ* is collinear with the straight-line *PK*, so it was obtained,

$$\frac{\boldsymbol{l}_{PQ}}{|\boldsymbol{l}_{PQ}|}=\frac{\boldsymbol{l}_{PK}}{|\boldsymbol{l}_{PK}|} \tag{12}$$

In Equation (12), $|\boldsymbol{l}_{QK}|=l_2$, $|\boldsymbol{l}_{PQ}|=\sqrt{l_1^2(\varphi_1)+h^2}$, and $|\boldsymbol{l}_{PK}|=\sqrt{l_1^2(\varphi_1)+h^2}+l_2$. According to Equation (12), $\boldsymbol{l}_{PK}$ can be calculated as follows:

$$\boldsymbol{l}_{PK}=\left|\frac{\boldsymbol{l}_{PK}}{\boldsymbol{l}_{PQ}}\right|\boldsymbol{l}_{PQ}=\left(1+\frac{l_2}{\sqrt{l_1^2(\varphi_1)+h^2}}\right)\boldsymbol{l}_{PQ} \tag{13}$$

According to Equation (9), $\boldsymbol{l}_{OK}=\boldsymbol{l}_{OP}+\boldsymbol{l}_{PK}$, so the coordinates of the center point *K* of the sieve can be expressed as

$$\begin{cases} K_x = P_x + l_{PKx} = -\dfrac{l_1(\varphi_1) l_2 \cos\alpha}{\sqrt{l_1^2(\varphi_1)+h^2}} \\ K_y = P_y + l_{PKy} = -\dfrac{l_1(\varphi_1) l_2 \sin\alpha}{\sqrt{l_1^2(\varphi_1)+h^2}} \\ K_z = P_z + l_{PKz} = h + \dfrac{h l_2}{\sqrt{l_1^2(\varphi_1)+h^2}} \end{cases} \tag{14}$$

where, l_{PKx}, l_{PKy} and l_{PKz} are the components of $\boldsymbol{l}_{PK}$ on the X, Y and Z axes.

In addition to the positions of the key points of the mechanism, it is also necessary to calculate the attitude angle of the sieve; in other words, the attitude of rod PQ must also be calculated.

When defining the attitude angle of the sieve, because the sieve in the vertical state needs to be rotated twice to obtain the current attitude of the sieve, the rotation angle around the Y-axis is defined as γ, and the rotation angle around the X-axis is defined as θ. Since the sieve does not rotate around the Z-axis, it is not necessary to calculate the rotation angle γ of the sieve around the Z-axis. The order of the angle reverse calculation is opposite to the order of the angle definition. It is necessary to find the rotation angle θ of the sieve around the X-axis first and then find the rotation angle γ of the sieve around the Y-axis.

If the PQ of the current attitude is rotated $-\theta$ around the X-axis, the rotated PQ will be on plane OXZ, and PQ becomes perpendicular to the normal of plane OXZ. Initially, $\boldsymbol{l}_{PQ}$=($-P_x$, $-P_y$, h), but after PQ rotates $-\theta$ around the X-axis, its coordinate becomes $\boldsymbol{l}_{PQn}$=(P_{nx}, O_y, P_{nz}), which is perpendicular to the normal of plane OXZ.

From the above, we first obtain:

$$\begin{bmatrix} 1 & 0 & 0 \\ 0 & \cos\theta & \sin\theta \\ 0 & -\sin\theta & \cos\theta \end{bmatrix} \begin{bmatrix} -P_x \\ -P_y \\ h \end{bmatrix} = \begin{bmatrix} P_{nx} \\ 0 \\ P_{nz} \end{bmatrix} \tag{15}$$

From Equation (15), we can proceed with:

$$-P_y \cos\theta + h\sin\theta = 0 \tag{16}$$

Therefore, the equation for the pitch angle will be:

$$\theta = \arctan\left(\frac{P_y}{h}\right) \tag{17}$$

Second, if $\boldsymbol{l}_{PQn}$ is rotated around the Y-axis by $-\gamma$, a vertical PQ will be obtained. Therefore, it was got,

$$\begin{bmatrix} \cos\gamma & 0 & -\sin\gamma \\ 0 & 1 & 0 \\ \sin\gamma & 0 & \cos\gamma \end{bmatrix} \begin{bmatrix} P_{nx} \\ 0 \\ P_{nz} \end{bmatrix} = \begin{bmatrix} 0 \\ 0 \\ P_{nnz} \end{bmatrix} \tag{18}$$

Simplifying Equation (18), it was obtained,

$$P_{nx}\cos\gamma - P_{nz}\sin\gamma = 0 \tag{19}$$

Therefore, the equation for the roll angle will be,

$$\gamma = \arctan\left(\frac{P_{nx}}{P_{nz}}\right) \tag{20}$$

In summary, when the coordinates of the sieve center point and the expressions of the two attitude angles of the sieve during the motion of the stirring mechanism are obtained, the establishment of the kinematics model is completed.

4.2 Reverse design of the stirring mechanism

4.2.1 Reverse of non-circular gear

Based on the kinematics model obtained above, the density of the sieve center points is controlled by non-circular gears. As shown in Figure 11, if the center point trajectory is projected on plane OXY and the origin is connected to each projection point, connecting lines will be obtained with different densities. The reason why the density of different connecting lines is different is that the rotation angle of the driven non-circular gear is different in unit time, and the included angle between these connecting lines is the corresponding rotation angle of the driven non-circular gear. The center points obtained above are projected to obtain the connecting lines of 360 points. The included angle between the connecting lines can be calculated to obtain the rotation angle of the driven non-circular gear.

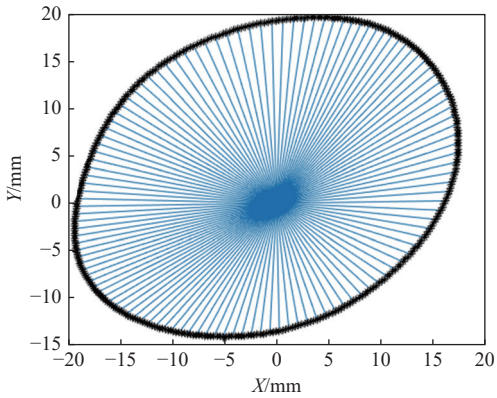

Figure 11 Schematic diagram of projected center point connecting lines

The driving wheel of the non-circular gear rotates at a constant speed, turning 1° at a time. Using the projected connecting line, the rotation angle of the driven wheel can be calculated. The trajectory of the sieve center point is known. Suppose the coordinate of the ith trajectory point K_i is denoted as (K_{xi}, K_{yi}, K_{zi}); then, the projected coordinate of the point K_i on the plane OXY is (K_{xi}, K_{yi}), and the included angle with the X axis is as follows:

$$\alpha_i = \arctan(K_{yi}/K_{xi}) \tag{21}$$

The angle α, included between the connecting lines of each center point and the x-axis is calculated by Equation (21), which is the angle where the connecting rod of the planetary gear train swings. Because the transmission ratio of the planetary gear train is 1, the angle α is equal to the rotation angle φ_2 of the non-circular driven gear. According to the angle relationship between the driving wheel and the driven wheel, the transmission ratio of the non-circular gear can be calculated using Equation (22) as follows:

$$i_{12} = \frac{\mathrm{d}\varphi_1}{\mathrm{d}\varphi_2} \tag{22}$$

In Equation (22), $\mathrm{d}\varphi_1$ is the change in the driving wheel's rotation angle, which is always 1°. $\mathrm{d}\varphi_2$ is the change in the driven wheel's rotation angle, which is calculated from the difference between the next included angle and the previously included angle.

The transmission ratio of the non-circular gear is calculated by Equation (22), and the radial diameter of the driving wheel and the driven wheel of the non-circular gear can be calculated by Equation (23), where a is the center distance of the non-circular gear as follows:

$$\begin{cases} r_1 = \dfrac{a}{1+i_{12}} \\ r_2 = a - r_1 \end{cases} \tag{23}$$

The following equation is used to convert the polar coordinate equation of the pitch curve into a rectangular coordinate equation.

$$\begin{cases} x_1 = r_1 \cos\varphi_1 \\ y_1 = r_1 \sin\varphi_1 \\ x_2 = r_2 \cos\varphi_2 \\ y_2 = r_2 \sin\varphi_2 \end{cases} \quad (24)$$

In Equation (24), (x_1, y_1) is the pitch curve coordinate of the driving wheel and (x_2, y_2) is the pitch curve coordinate of the driven wheel.

Let the center distance a of the non-circular gear be 160 mm; the pitch curve of the non-circular gear is obtained by reverse calculation, and the pitch curve is further optimized[25-27]. Finally, the pitch curve and tooth profile of the non-circular gear are obtained, as shown in Figure 12.

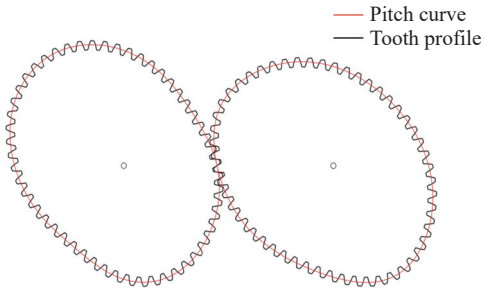

Figure 12 Pitch curve and tooth profile of non-circular gear

4.2.2 Reverse of the cam

Given the center point of the spherical hinge and the cone apex point, the attitude of the sieve can be determined, and the position of the center point of the spherical hinge is completely controlled by the cam. According to the kinematic model of the mechanism, the sieve center point, the cone apex point, and the center point of the spherical hinge are collinear. The coordinates of the sieve center point and the cone apex point are known, and the center point of the spherical hinge is always in the same plane perpendicular to the Z-axis. Suppose that the center point of the spherical hinge moves on the plane $z=-h$, and the coordinate of the ith center track point of the sieve is consistent with the above (K_{xi}, K_{yi}, K_{zi}).

According to the collinearity of the sieve center point, the cone apex point, and the center point of the spherical hinge, Equation (25) can be obtained, and l_{OPi} in Equation (26) indicates the distance from the cone apex point O to the center point of the spherical hinge.

$$\frac{\sqrt{K_{xi}^2 + K_{yi}^2}}{l_{OPi}} = \frac{K_{zi}}{h} \quad (25)$$

$$l_{OPi} = \frac{h\sqrt{K_{xi}^2 + K_{yi}^2}}{K_{zi}} \quad (26)$$

Considering the size of the slider, suppose the distance from the center point of the spherical hinge to the contact point of the slider and the cam is d_{hk}, and the center distance between the two gears in the planetary gear train is A. Hence, the radial diameter ρ_i of the cam can be expressed as in Equation (27).

$$\rho_i = A - l_{OPi} - d_{hk} \quad (27)$$

The cam is fixed to the driven non-circular gear, so the rotation angle of the cam is also φ_2. Based on the cam's radial and rotation angles, the cam profile equation converted from polar coordinates to rectangular coordinates can be expressed as follows:

$$\begin{cases} x_3 = \rho \cos\varphi_2 \\ y_3 = \rho \sin\varphi_2 \end{cases} \quad (28)$$

By adjusting the parameters of the mechanism, a set of better cam parameters is obtained as h=200 mm, A=200 mm, and l_{hk}= 20 mm. The cam profile is calculated and optimized based on the above equation, and the final cam profile is shown in Figure 13.

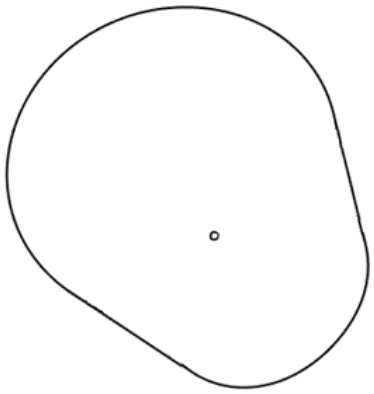

Figure 13 Cam profile of cam slider mechanism

4.3 Stirring mechanism auxiliary analysis and design software

According to the established kinematics model and reverse model of the variable-speed and variable-amplitude stirring mechanism, the auxiliary analysis and design software was written using MATLAB software, for which the GUI is shown in Figure 14. The software is easy to operate, and the reverse result can be quickly acquired by inputting the mechanism parameters through the GUI. By adjusting the mechanism parameters, the changes in the non-circular gear pitch curve and the cam profile can be visualized, which is convenient for the analysis and design of the mechanism. The software can also display the motion simulation animation of the stirring mechanism under the reversed parameters and output the change in the sieve attitude angle during the stirring process. According to the non-circular gear pitch curve and cam profile curve displayed by the software, combined with the comparison between the rotation angle curve obtained by the motion simulation and the theoretical rotation angle curve, it can be determined whether the current mechanism meets the design requirements to obtain satisfactory mechanism parameters.

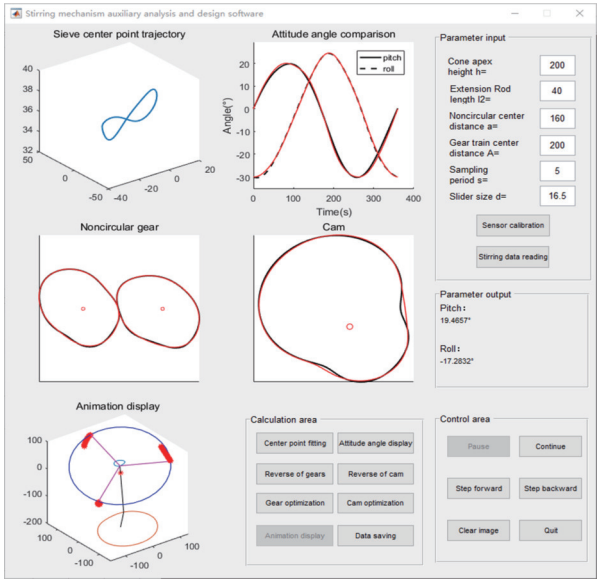

Figure 14 Interface of the stirring mechanism auxiliary analysis and the design software

5 Design, simulation, and experiment of the oolong tea stirring machine

Based on the determined parameters of the stirring mechanism, a three-dimensional model of the variable-speed and variable-

amplitude stirring mechanism was established, and ADAMS was used for simulation analysis. Finally, a prototype was built for the experiment to further verify the feasibility of the mechanism.

5.1 Whole design of the oolong tea stirring machine

The three-dimensional design of the oolong tea stirring machine was carried out, and the three-dimensional model is shown in Figure 15.

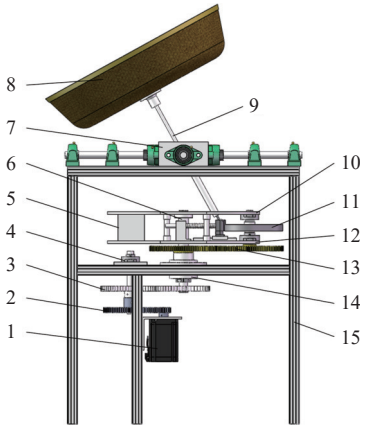

1. Stepper motor 2. Reduction gear 3. Non-circular gear 4. Double bearing seat 5. Counterweight 6. Main shaft 7. Shaking frame 8. Bamboo sieve 9. Sieve shaft 10. Upper plate 11. Cam mechanism 12. Lower plate 13. Planetary gear train 14. Flange bearing seat 15. Frame

Figure 15 Three-dimensional diagram of the stirring machine

The oolong tea stirring machine is mainly composed of a frame, a cam mechanism, and a transmission assembly. Among them, the structure of the frame is the same as that of the test bench, and it is also composed of a frame, a shaking frame, a bearing set, a sieve shaft, and a sieve, which provides a fixed cone apex point for stirring. The cam assembly provides a moving spherical hinge point for stirring, which cooperates with the fixed cone apex point to determine the attitude of the sieve, and its motion is driven by the main shaft and planetary wheels. The transmission component is composed of a stepping motor, a reduction gear, a non-circular gear, a bearing seat, and a planetary gear train, which provides power for the entire machine.

The working principle of the machine is as follows. The stepping motor outputs a constant speed motion, drives the reduction gear and the non-circular gear to rotate, and then transmits the power to the main shaft for rotation. The main shaft drives the upper and lower plates to rotate and then drives the planetary gear to rotate around the sun gear to transmit power to the cam. The cam pushes the slider to move along the linear guide, so the spherical hinge revolves around the sun gear while sliding with the slider and cooperates with the fixed cone apex point to determine the attitude of the sieve. The revolution speed of the spherical hinge around the sun gear is controlled by the non-circular gear; therefore, the shaking speed of the sieve is controlled by the non-circular gear. The linear motion of the spherical hinge is controlled by the cam; that is, the shaking amplitude of the sieve is controlled by the cam.

5.2 Virtual simulation, development, and experiment of the oolong tea stirring machine

To verify the accuracy of the reverse-designed variable-speed and variable-amplitude stirring mechanism, the ADAMS was used to establish a virtual prototype model. After importing the 3D model of the machine, the kinematic pair for the components was added, the material properties were set, the driving and force were added, and finally, the simulation was performed. The rotation angles of the two rotating shafts were measured in ADAMS. Due to the different reference standards of the software, the data were processed in MATLAB software to obtain the two-axis simulation rotation angle curve.

According to the three-dimensional design of the oolong tea stirring machine, the parts of the prototype were processed, and the assembly of the whole machine was completed. Figure 16 shows the diagram of the prototype. In addition to completing the construction of the oolong tea stirring machine, a data acquisition system for collecting the attitude angle of the sieve was installed on the prototype. The data collection method of the prototype is consistent with the test bench.

1. Frame 2. Shaking frame 3. Bamboo sieve 4. Hall angle sensor 5. Cam mechanism 6. Non-circular gear 7. Stepper motor

Figure 16 Diagram of the oolong tea stirring machine prototype

To verify whether the machine meets the attitude requirements of stirring, the rotation angle of the two shafts during stirring must be obtained through the stirring test. The sensor of the prototype was calibrated, and then the stirring data collection test of the machine was completed. The collected rotation angle data were imported into MATLAB for processing. Figure 17 shows the comparison between the simulation rotation angle curve obtained by ADAMS, the actual rotation angle curve collected by the prototype, and the theoretical rotation angle curve.

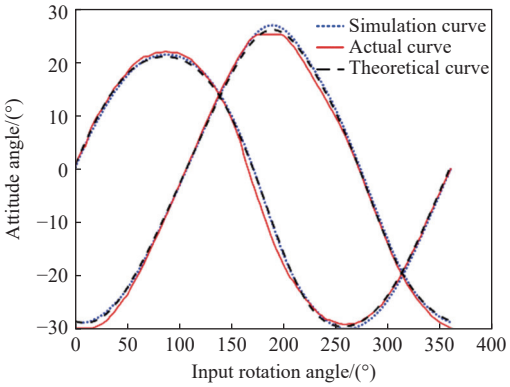

Figure 17 Comparison of the simulation, actual, and theoretical rotation angle curves

In Figure 17, the dashed line is the theoretical rotation angle curve, the dotted line is the simulated rotation angle curve, and the solid line is the actual rotation angle curve. Among them, the simulation curve and the theoretical curve have a slight deviation, and except for individual areas, they are basically similar, which in turn verifies that the designed mechanism can reproduce the target rotation angle curve. Exploring the reasons for the deviation between the simulated curve and the theoretical curve, the following reasons may be outlined as contributors. First, because the non-

circular gears and cams obtained by the reverse calculation are optimized, which are different from the results obtained by the direct reverse calculation, there is a difference in the simulation results that were obtained. Second, because non-circular gears transmit motion through tooth profile meshing, the non-circular tooth profile generated by software has errors and cannot fully follow the designed transmission ratio. Third, ADAMS may have errors in its simulation results due to settings and accuracy.

Compared with the theoretical curve, the actual curve fluctuates in some areas, but the overall trend is basically the same. Through the analysis and comparison of the actual curve data and the theoretical curve data, the maximum deviation of the pitch angle is 2.8772°, and the maximum deviation of the roll angle is 1.5948°. It can be considered that the actual curve is basically consistent with the theoretical curve, which verifies the accuracy of the designed stirring mechanism. The difference between the actual curve and the theoretical curve may be due to the following reasons. First, the error in part processing may lead to a difference between the actual output characteristics and theoretical output characteristics of non-circular gears and cams, resulting in a deviation between the actual curve and the theoretical curve. Second, because of the assembly errors of the machine, the actual installation position or phase of the parts may be inconsistent with the design, resulting in an error between the actual and theoretical curves. Third, the torque change in the motion process may lead to the uneven output speed of the motor, which brings errors. Fourth, the vibration caused by the cam offset may affect the stability of the machine, resulting in deviation in the test results. Overall, the rotation angle curves of the experiment and theory are basically consistent, which verifies the correctness of the reverse design and modeling of the stirring mechanism and shows that the stirring mechanism can meet the working requirements.

As shown in Figure 18a, fresh tea picked in Songyang, Lishui without stirring was tested on the stirring machine based on the local stirring process. The specific stirring process parameters are as follows. The rotating speed of the stirring machine was 40 r/min, and the stirring was divided into four stages. After stirring for 4 min and drying for 1.5 h for the first time, stirring for 5 min and drying for 1.5 h for the second time, stirring for 20 min and drying for 2.5 h for the third time, and stirring for 30 min and drying for 6 h for the fourth time, the final tea is shown in Figure 18b. Compared with the tea before and after stirring, the tea before stirring is fresh, tender, and green. After stirring, the tea collides and rubs, and the red edge appears on the leaf edge, forming an obvious “green leaf with a red edge”, and the tea emits an aroma. The experimental results show that the oolong tea stirring machine can stir fully and evenly.

a. Tea before stirring

b. Tea after stirring

Figure 18 Comparison of the tea before and after stirring

6 Conclusions

First, based on the field investigation, the requirements of manual stirring motion characteristics of oolong tea were summarized. A manual stirring motion characteristic collection test bench was designed, and the manual stirring motion characteristics were collected. The motion characteristics of standard manual stirring were expressed based on a Fourier series.

Second, the variable-speed and variable-amplitude stirring mechanism was designed, the kinematic model and reverse design model of the stirring mechanism were established, the auxiliary analysis and design software were written, and the non-circular gear pitch curve and cam profile curve of the stirring mechanism were obtained.

Finally, the oolong tea stirring machine was designed and then simulated by Adams, a prototype of the stirring machine was developed, and a stirring data collection test was carried out. By comparing the theoretical curve, simulation curve, and actual curve, it was found that the curves were basically consistent, which verifies the correctness of the design of the stirring mechanism. Tea stirring experiments were carried out, which proved the feasibility of mechanical stirring by the designed stirring machine.

Acknowledgements

The authors acknowledge that this work was financially supported by the National Natural Science Foundation of China (Grant Nos. 51975536 and U23A20175) and the China Agriculture Research System of MOF and MARA. The authors also acknowledge American Journal Experts for their language assistance during the preparation of this article.

[References]

[1] Li Y H. Discussion on the traditional primary processing technology of Anxi Meizhan oolong tea. Journal of China Tea Processing, 2016; 2: 57–59,63. (in Chinese)

[2] Wei Z C, Lin D C, Yu X L, Xiang Y P, Lin H Z, Hao Z L. Research progress on intelligent greening technology for Oolong tea. Subtropical Agriculture Research, 2021; 17(1): 34–39. (in Chinese)

[3] Xie W H. How to master the oolong tea green-making technology. Tea in Fujian, 2008; 2: 27–28. (in Chinese)

[4] Zhang R M. Analysis of Green Technology of Oolong Tea. China Food Safety Magazine, 2022(16): 145–147. (in Chinese)

[5] Jin X Y. Tea processing engineering. Beijing: China Agricultural Press. 2014; 300p. (in Chinese)

[6] Jin X Y, Ji K W, Guo Y L. Application of mechanical vibration in the rocking process of oolong tea. Journal of Tea Science, 1994; 14(2): 149–154. (in Chinese)

[7] Hao Z L, Chen J B, Jin X Y, Lin Q J, Huang Y B. Development and performance test of fine manipulation environment control for oolong tea

vibrating fine manipulation equipment. Transactions of the Chinese Society of Agricultural Engineering, 2013; 29(10): 269–277. (in Chinese)

[8] Cheng D M, Shen M X, Huang M Q, Lin Y P. Hand-sieve type moving tea greenness deleting machine. CN. Patent number. ZL201127259. 2008.10. 08. (in Chinese)

[9] Yang J, Liu M H, Ruan C Z, Zhang B, Ye J H. Design of spherical type 360° of tea stirring machine, flow field analysis and experimental analysis. Food & Machinery, 2020; 36(10): 81–86. (in Chinese)

[10] Cai Z X, Xie B. Robotics. Beijing: Tsinghua University Press. (3rd ed.). 2022; 207p. (in Chinese)

[11] Fan Y Y, Zhao B. Coordinate measurement of hidden parts using an attitude angle sensor and a laser rangefinder. Optical Engineering, 2014; 53(12): 124101.

[12] Zhu Y H, Yang H, Li R, Zhang Y J, Chen Q, Hua Y S, et al. Wireless detector for translational and rotational motion of spherical-particle flow. Powder Technology, 2020; 360: 882–889.

[13] Ren L, Wang N, Cao W B, Li J Q, Ye X C. Trajectory planning and motion control of full-row seedling pick-up arm. International Journal of Agricultural and Biological Engineering, 2020; 13(3): 41–51.

[14] Li X G, Wei S M, Liao Q Z, Zhang Y. A novel analytical method for four-bar path generation synthesis based on Fourier series. Mechanism and Machine Theory, 2020; 144: 103671.

[15] Sun J W, Chu J K. Fourier series representation of the coupler curves of spatial linkages. Applied Mathematical Modelling, 2010; 34: 1396–1403.

[16] Bloomfield P, Bloomfield J E. Fourier analysis of time series: An introduction. (2nd Ed.). Nueva Jersey: Hoboken, 2000; 286p.

[17] Stein E M, Shakarchi R. Fourier analysis: An introduction. Princeton University Press, 2002; 320p.

[18] Chu J K, Sun J W. Unified approach to synthesis of coupler curves of linkage by fourier series. Journal of Mechanical Engineering, 2010; 46(13): 31–41.

[19] Sun J W, Chu J K. Synthesis of coupler curves of spatial linkage through Fourier transforms. Machine Design & Research, 2008; 2: 28–30. (in Chinese)

[20] Tong Z P, Yu G H, Zhao X, Liu P F, Ye B L. Design of Vegetable Pot Seedling Pick-up Mechanism with Planetary Gear Train. Chinese Journal of Mechanical Engineering, 2020; 33(63): 1–11.

[21] Litvin F L, Gonzalez-Perez I, Fuentes A, Hayasaka K. Design and investigation of gear drives with non-circular gears applied for speed variation and generation of functions. Computer Methods in Applied Mechanics and Engineering, 2008; 197(45-48): 3783–3802.

[22] Gao Q F, Ye J, Liu C. Design and modeling of noncircular gear with curvature radius function. Journal of Computational Methods in Sciences and Engineering, 2018; 18(3): 683–693.

[23] Yu G H, Tong Z P, Sun L, Tong J H, Zhao X. Novel gear transmission mechanism with twice unequal amplitude transmission ratio. Journal of Mechanical Design, 2019; 141(9): 092304.

[24] Ottaviano E, Mundo D, Danieli G A, Ceccarelli M. Numerical and experimental analysis of non-circular gears and cam-follower systems as function generators. Mechanism and Machine Theory, 2007; 8(43): 996–1008.

[25] Ye B L, Yi W M, Yu G H, Gao Y, Zhao X. Optimization design and test of rice plug seedling transplanting mechanism of planetary gear train with incomplete eccentric circular gear and non-circular gears. International Journal of Agricultural and Biological Engineering, 2017; 10(6): 43–55.

[26] Zhu Z F, Wu G H, Ye B L, Zhang Y C. Reverse design and tests of vegetable plug seedling pick-up mechanism of planetary gear train with non-circular gears. International Journal of Agricultural and Biological Engineering, 2023; 16(2): 96–102.

[27] Xu H, Fu T W, Song P, Zhou M J, Fu C W, Mitra N J. Computational Design and Optimization of Non-Circular Gears. Optimization for Fabrication, 2020; 39(2): 399–409.